ACS APPLIED ELECTRONIC MATERIALS

pubs.acs.org/acsaelm Review

Resists for Helium Ion Beam Lithography: Recent Advances

Nagarjuna Ravi Kiran, Manvendra Chauhan, Satinder K. Sharma, Subrata Ghosh,* and Kenneth E. Gonsalves*

Cite This: https://dx.doi.org/10.1021/acsaelm.0c00627 Read Online

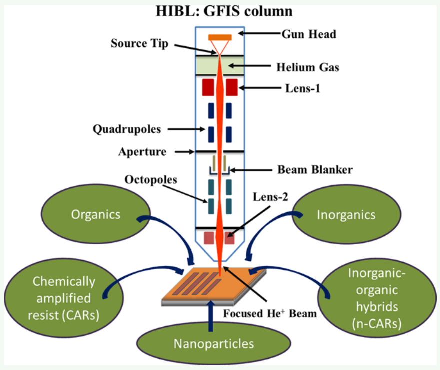

ABSTRACT: Since the fabrication of micro-/nanoelectronic devices are marching toward ultralow node technology with dense patterns to meet the current industry demands, continuous advancement is needed in terms of material design and lithographic techniques. In this perspective, helium ion beam lithography (HIBL) has gained tremendous attention of the scientific society to realize high-performance device fabrication with advanced technology. Salient features of the helium ion beam including sub-nanometer spot size, high-intensity lighter ion (with respect to gallium and neon ions) make the HIBL technique a competitive next-generation lithography tool. This review describes, in brief, the significance of HIBL technology in comparison with electron beam lithography (EBL); however, it presents in detail the development made in the area of resists for HIBL. One of the important characteristics of He^+ beam is, reduced backscattering leads to minimizing the proximity effects in contrast with EBL. Furthermore, it emphasizes the developments of various resist materials to perform high-resolution patterns at comparable line-edge roughness/line-width roughness (LER/LWR) values. HIBL performances of various classes of materials are presented here to give a overall conception of the technique. The materials including organic, inorganic, organic−inorganic hybrids, and nanoscale materials which have shown promising patterning under He^+ beam irradiation have been included and discussed in this work.

KEYWORDS: *helium ion beam lithography, electron beam lithography, next-generation lithography, proximity effect, high resolution, LER/LWR, spot size*

1. INTRODUCTION

1.1. Lithographic Techniques. Fabrication of micro-/nanoelectronic devices has become an inevitable need to meet several requirements of modern life.[1,2] Several lithographic techniques have been developed and implemented to fabricate these devices that include photolithography, electron beam lithography, soft lithography, nanoimprint lithography (NIL), electro-hydrodynamic lithography, direct-write assembly, selective surface wetting, dip-pen nanolithography, and so on.[3−10] Each and every technique possesses its own merits and demerits. Basically, lithography is the process of making repetitive units as a pattern in a layer of material, called resist, with the help of radiation-induced chemical reactions. Further, this pattern is transformed into the functional layer by etching or lift-off process.[11] As per the recent trend of the nanofabrication, extreme ultraviolet (EUV) is considered to be the most effective next-generation lithography (NGL) technique due to its capability to create lower (sub-∼10 nm) node patterns with high resolution.[12,13] In addition to conventional lithography tools, various alternate lithographic techniques are emerging into the research and production fields of nanoelectronics. Among those, electron beam lithography (EBL) is one of the tools which is a direct-write method by exposing the resist with a focused electron beam. EBL has been successfully shown to have the potential for fabricating features with sizes below 10 nm.[14] In line with EBL, another class of maskless lithographic techniques is helium ion beam lithography (HIBL).[15,16] The HIBL comes under the technique called focused ion beam (FIB) lithography. HIBL utilizes the lighter ion beam of helium and centers on resist material to bring the required chemical changes in order to create the patterns in the thin film. In comparison with EBL, HIBL has also demonstrated a significant narrow scale patterning.[17] The above-mentioned three tools proceed through the analogous operational mechanism. In typical photolithography, a photosensitive material is irradiated with ultraviolet radiation to produce the desired shape and dimension, whereas, in the case of EBL and HIBL, an electron/ion-sensitive resist is exposed with electron/ion beam, respectively.[12,18]

Received: July 19, 2020
Accepted: October 22, 2020

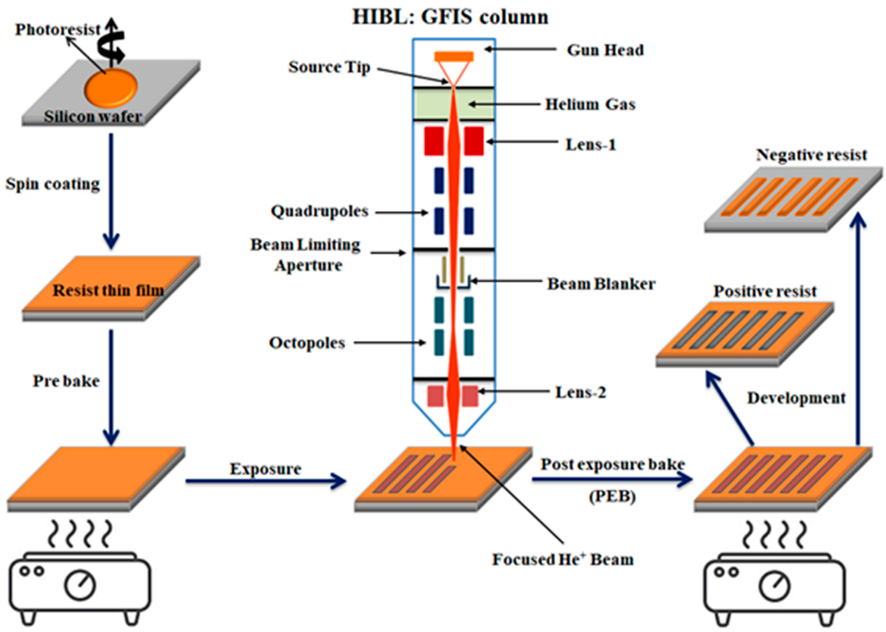

Figure 1. Schematic representation of the helium ion beam lithography process.

The outline of the process of the helium ion beam lithography technique is depicted in Figure 1. The formulated photoresist solution is spin-coated over a silicon substrate with adequate rpm and time to generate a defect-free thin film of required thickness. Later, the thin film is subjected to a pre-exposure bake on a hot plate to remove the residual solvent in it. After the prebake process, the resist thin film is irradiated with an ion beam according to the required pattern. Then the exposed thin film is placed on the hot plate, which is known as a postexposure bake (PEB). The ion-induced reactions in the resist film, leads to the formation of soluble and nonsoluble material in a particular solution. The soluble areas get dissolved in the developer solution, and nonsoluble areas remain undissolved to produce the patterns; this process is called resist development. On the basis of the solubility of the ion-sensitive material after exposure, the resist solutions are classified into two types: positive and negative resists. In the case of positive resists, the irradiated portion undergoes a chemical reaction to yield easily soluble material and the nonirradiated portion does not suffer from any chemical change. Hence, the unexposed region stays as patterns and the exposed area gets dissolved away in the developer solution. On the other hand, in the case of negative resist, the exposed area stays back on the substrate after developing while the unexposed area gets dissolved away, and thereby patterns are created due to exposed regions.

1.2. Terminology. The common terminologies that have been repeatedly mentioned in this review are expanded below. These terminologies are used to describe the properties and performance of the resist materials and techniques associated with various lithography processes.

Dose: This is a quantitative factor of incident energy. The dose can be varied by changing the beam current, dwell time, and pixel spacing.

Sensitivity: It is defined as the minimum exposure dose which is required to initiate the desirable chemical reactions in the resist thin film.

Throughput: Throughput is said to be the number of features produced per second. This term is an indication of the speed of the lithographic process.

Proximity effect: An unintended exposure of the beam on the surrounding area of the interested region or an incident area. This effect is caused due to primarily backscattered electrons/ions from substrate.

Contrast: A contrast of the exposed photoresist describes the remaining fraction of the photoresist after development as a function of the exposure dose. It also vitally relies on all of the photoresist processing steps.

Resolution: It is known to be the reproducibility of minimum size features with a distinct differentiation.

2. SIGNIFICANCE OF HIBL

2.1. Why Helium Ion Beam Lithography? The lithographic techniques are classified into two categories on the basis of the patterning process such as parallel and serial lithography.[19] For parallel lithography, a suitable mask is used to focus the beam through it to get the required pattern on the resist thin film, whereas, in serial lithography, the beam of the charged particle is directly focused point-by-point (raster scan) on the resist to write the pattern.[20] Examples of the serial lithographic techniques are EBL, FIB, and so on.[19] Though EBL has been demonstrated for the rapid development of prototypes for new devices, it is limited by long-range proximity effects at higher energies above 30 keV. This effect is due to backscattered electrons (BEs) produced in the resist with high-energy radiation.[21] The backscattered electrons further interact with some more material in the proximity of the scanned region. In addition to BEs, the forward scattering also plays an important role in determining the minimum feature size of the written pattern in EBL. This influence leads to the chemical changes in the unexposed region too.[19] Therefore, the pattern size is wider than that of the exposed pattern area, while in FIB a much lower number of ions undergo backscattering which does not lead to long-range proximity effects.[19,22] In another aspect, EBL proceeds through the generation of low-energy SEs to initiate the chemical or physical reactions in the resist material, but, in FIB, a greater number of SEs are produced compared to those in EBL in order to accelerate the process with minimal forward and backscattering mechanism.[22,23] Hence FIB is considered to be more efficient than EBL for high-resolution patterning.[19] HIBL also has an advantage in terms of producing high-density patterns. In general, EBL has been proven to have capability in patterning sub-10 nm isolated lines and arbitrary features; however, reports on well-resolved sub-10 nm dense features are limited, possibly due to critical proximity concerns.

As discussed, FIB has the ability to fabricate the patterns with a resolution comparable with probe size.[19] However, with heavier ions, such as gallium and neon, the resolution is not comparable with EBL due to large beam spot size.[24,25] Other drawbacks of heavy ions beam exposures are substrate damage and the resist contamination by ion influence.[26] These issues restrict the use of heavy ions beam lithography for high-resolution nanoscale patterning. On the other hand, lighter ions such as helium can achieve desirable features with a resolution similar to that with EBL or better. Around two decades ago, gas field ion source (GFIS) using helium ion was established for ~200 nm resolutions.[27] In recent times, various developments have been carried out for HIBL in terms of the source of light ion beam and column configuration made the spot size less than sub-nanometer (≤0.35 nm).[16,28] These developments are also resulting in a considerable decrease in the sample damage. The short ion range (spot size) is useful to reduce the diffusion of SEs to adjacent areas, and therefore, the resolution will be improved.[15] Also, the proximity effect was reduced to 50 times using He^+ ion beam in comparison to e-beam interaction with the resist sample.[29] Due to these advancements, it is anticipated that the HIBL can compete with the resolutions of well-demonstrated EBL.

2.2. Advantages of HIBL. *2.2.1. Maskless Approach.* Similar to EBL, it helps with good flexibility in writing arbitrary patterns, whereas other lithographic tools need the mask to be fabricated and the radiation through the mask has to be passed out. This is time-consuming as well as an expensive process. Hence, this tool is efficient and offers a low-cost-patterning solution for low-volume or single-item features.[19]

2.2.2. Diameter of Focused Beam. The sub-nanometer spot size of the beam (≤0.35 nm) determines the resolution of HIBL patterns.[30] The resolution depends on the diameter of the focused beam rather than the wavelength of the radiation.[19]

2.2.3. High-Density Patterning. Because the proximity effect is minimized in HIBL compared to EBL, eventually the number of distinct and low size patterns per area formation will be increased. This in turn leads to formation of a high-density pattern array.

2.3. Disadvantages of HIBL. Using a tool with a parallel exposure technique, for example, EUV stepper, 193 immersion lithography, and deep ultraviolet lithography, etc., a large-area exposure of the resist film is achieved and therefore employed for high-volume patterning for bulk production in less time. At the same time, HIBL is a serial patterning technique, which is more time-consuming in terms of writing time and good for prototyping of high-resolution patterning in comparison with parallel exposure methods. Moreover, a charged particle beam for such serial-writing tools is the function of dose as well as the required pattern area. Hence, with the shrinking of device feature size the prerequisite of the dose will increase to approach the state of the art LER/LWR values.[31] This is where HIBL is limited by low-throughput patterning.[32] Thus, HIBL is most suitable for patterning of a single item, low-volume features.

3. HIBL INSTRUMENTATION

The instrument of focused helium ion beam consists of three major components. They are gas field ion source (GFIS) gun, column, and process chamber as shown in Figure 2.[19]

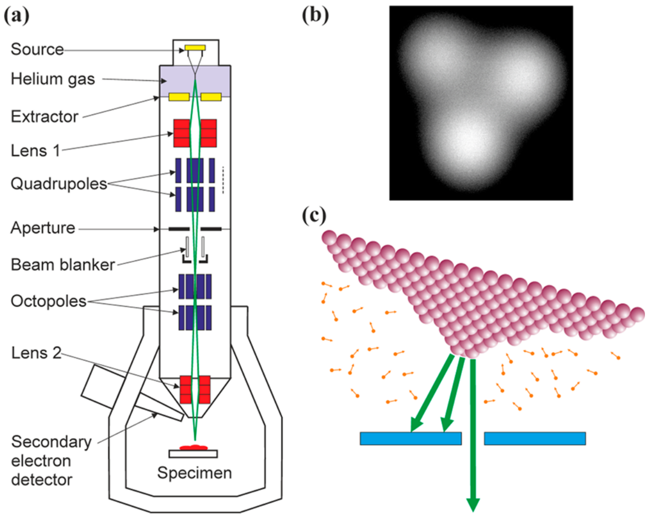

Figure 2. (a) Schematic of a helium ion beam system, showing the ion source, column, optics, and sample chamber. (b) Image of the trimer containing three atoms at the top of the pyramid of a tungsten tip, where ionization occurs and three beams of helium ions are generated. (c) GFIS emitter tip region. Neutral helium atoms (orange) are ionized at the emitter forming three beams of helium ions (green). They are accelerated away from the tip and one of them is aligned to the axis of the column and focused on the sample in the chamber. Reprinted with permission from ref 19. Copyright 2016 Elsevier.

3.1. Gas Field Ion Source Gun. It sits at the top of the GFIS column and includes a source and the extractor. Tungsten wire is used as the source mounted at the top of the column, in the gun assembly; the apex of the source tip acts as an emitter of ions. This end of the wire consists of a pyramidal-shaped tip with an apex of three tungsten atoms. Specifically, this arrangement is called as "trimer". Such atomic-level configuration can be precisely controlled by high electric fields and also can be monitored using the scanning field ion microscopy (SFIM) operational mode of the system. The helium gas ionizes at the uppermost atoms of the pyramid due to a strong electric field created between the positively biased source and the extractor with the negative voltage. The resulting ion beam passes through the hole in the middle of a circular plate that mounts just below the source, called the extractor plate. Basically, the generated beam from the preferred brightest atom among the three is aligned with the column line which produces the ideal point source. This phenomenon makes the source to have a narrow source size, smaller energy spread, and greater brightness. Further, this function leads to allow the column to operate with less demagnification and small beam convergence angle and finally helps in a long depth of focus for the imaging of the pattern.[19]

3.2. Gas Field Ion Source Column. The generated helium ions (He^+) at the tip of the electrode then accelerated

https://dx.doi.org/10.1021/acsaelm.0c00627
ACS Appl. Electron. Mater. XXXX, XXX, XXX−XXX

into the column. The column is a traditional two-lens (lens 1 and lens 2) electrostatic configuration, along with beam deflectors (quadrupoles and octopoles) and beam-limiting apertures. The diverged ion beam crosses through the extractor plate, converged by lens 1 at a certain point, which then directed on-axis with the center of lens 2 using quadrupoles. The adjustments to the quadrupole plate's voltages can be made during beam-limiting-aperture alignments, while the aperture is located in the middle of the column. It is a disk-like shape with an orifice that helps to allow the center of the beam to pass through the column. After the aperture, a beam blanker is arranged to steer the beam toward the sample. As the name suggests, the beam blanker is used to blank the beam and measure the ion beam current as required by applying equal and opposite voltages to the plates of the blanking aperture. After crossing the beam blanking aperture, the ion beam encounters the octopoles. The signals applied to the octopoles by controlling the parameters such as the field of view and the image size (pixels) cause the deflection of the ion beam to scan across the target. Lastly, the ion beam is managed by the last element of the GFIS column, lens 2, to focus onto the target. The voltage across lens 2 can be controlled by adjusting the focus through a knob present on the panel. The GFIS gun as well as the column are operated under high vacuum ranging from 10^{-9} to 10^{-10} Torr, to avoid interference from other gas particles or ions.[19]

3.3. Process Chamber. The samples are set in the process chamber, which is seated at the base of the apparatus, beneath the column. The chamber is comprised of the stage, cradle and tilt assembly, camera, a flood gun, and several signal detectors, such as an Everhart−Thornley (ET) detector, to collect emitted SEs and an optional microchannel plate (MCP)/silicon drift detector to utilize backscattered He^+ from the sample surface. It is maintained at a high vacuum of typically $\sim 10^{-7}$ Torr, and the helium ion beam is focused on the sample to the pattern in a definite manner per the requirements.[19]

4. HELIUM ION−MATERIAL INTERACTION

4.1. Interaction Volume. Interaction volume is known as the predictable volume of the sample which is excited and affected by the primary beam. The shape and size of this are determined by the factors such as the type of charged particle, the angle and the energy of the incident beam, and the composition of the resist material (mass and density). As depicted in Figure 3, the He^+ beam penetrates deep into the sample before it diverges compared to Ga^+ and electron beams.[15] At this time, the generated secondary electrons (SEs) do not escape and the interaction of SEs with the material is constrained to lesser volume.[15] This phenomenon was studied using Monte Carlo simulation for three different charge particle beams—Ga^+ beam (at 30 keV), low-energy e-beam (at 1 keV, generally preferred over high-energy e-beam to reduce proximity effect comparatively), and He^+ beam (at 30 keV)[15,19] —which evidently proved that the interaction of a focused He^+ beam with the target sample is significantly lower in comparison to the other two competitive charged particle beams.[19]

As soon as the beam of irradiation particles hits the sample, the chain of reactions starts to occur on the basis of the composition of the material. This interaction takes place not only at the point of the incident but also deep into the material (Figure 4).[17,19] The distribution of generated SEs depends upon the interaction volume of the irradiated beam over the

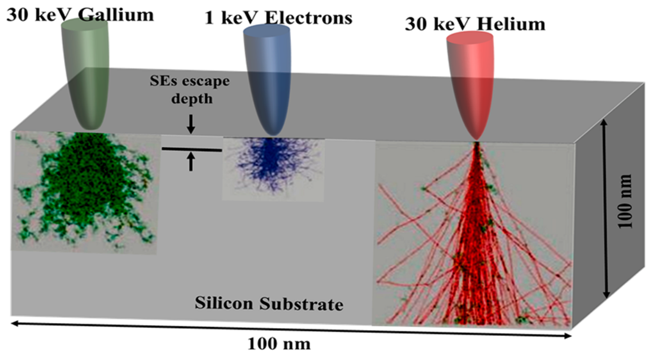

Figure 3. Monte-Carlo modeling results for representative beams into silicon. Near the surface, where secondary electrons can escape, the helium beam produces a very narrow excited volume. Hence the helium image contains surface information about the probed area.. Reprinted with permission from ref 15. Copyright 2007 AIP Publishing (to improve image resolution, the figure has been modified to 3D by taking the interaction volume from the original figure).

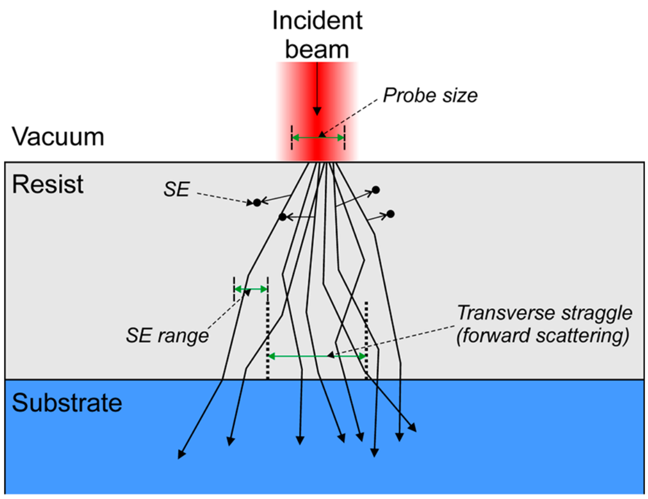

Figure 4. Schematic of the interactions of primary energetic He^+ ion beam with a resist layer on the silicon substrate, showing the production of secondary electrons, which is the main driver for the resist exposure. Three factors limiting the lithographic resolution are the spot size of the beam, ion scattering, and secondary electron emission. Reprinted with permisson from ref 19. Copyright 2016 Elsevier.

sample. If the interaction volume is less, then the generated SEs are constrained to a small area which allows a high resolution.[33] In the case of HIBL, the SEs are generated from the cylindrical interaction volume at the He^+ beam penetration point with a diameter $\sim$ 1 nm and an effective diffusion length $\leq$ 3 nm. Such a small probe volume assists with accomplishing extremely high resolution in HIBL.[34] Since the helium ion is lighter than its present competitive sample nuclei and heavier than electrons, it does not deflect from the original path of the beam. Hence the helium ions penetrate considerably into the sample before even they disperse. This outcome leads to a decrease in the backscattering and ultimately a decrease in the proximity effect in contrast to EBL and results in high-resolution dense patterning.[35]

4.2. Secondary Electron Generation. The mechanism for the generation of SEs during the process of ion beam lithography is similar to EBL. In both, primary particles generate low-energy SEs and are responsible for bond-breaking

https://dx.doi.org/10.1021/acsaelm.0c00627
ACS Appl. Electron. Mater. XXXX, XXX, XXX−XXX

or cross-linking reactions. However, the helium ion beam produces more SEs compared to electron beam. Because of the higher mass of He^+ ion than that of electron, a small amount of He^+ beam energy is sufficient to excite more electrons on collision. On an average, 2−8 SEs can be generated from each of He^+ particles.[19] But the number of SEs in EBL is 0.5−1.25 by each of the incident electrons.[15,36] Further the high yield of SEs helps in improving the signal-to-noise ratio (S/N) for better imaging. Different materials produce different numbers of SEs and allow the imaging with good contrast for superior resolution.[37]

4.3. Exposure Dose−Sample Damage. Since the ions have a much larger momentum compared to electrons, they can cause more damage to the sample. In the case of He^+ ions, they are lighter than Ga^+ ions and therefore can be utilized as a source for many FIB processes.[19] So He^+ ion has less impact on the sample, allowing less material contamination. At the same time, He^+ ion shows low ion backscattering that helps in deep penetration into the sample. Typically the penetration depth of 30 keV He^+ ions is several hundreds of nanometers. But the common thickness of the resist is in the range of 10−100 nm scale. So, the ion beam can penetrate into the underlying material, substrate, and cause the damage. When the dose of the ions is high, then the ion-induced damage zone can be formed, which can result in altering the material properties, surface swelling, amorphization, and bubble formation.[38,39] To circumvent this issue, the dose has to be optimized during HIBL process. Livengood et al. studied the experimental damage volumes as a function of ion dose with Monte Carlo simulations using the SRIM software package.[38] The investigations showed that the negligible physical damage is observed with a dose ~10 μC/cm^2.[38]

5. RESIST MATERIALS FOR HIBL

Several He^+ beam sensitive materials were reported in the literature including organic, inorganic, hybrid organic−inorganic, and nanoscale materials.

5.1. Organic Resists. Various classes of materials have been investigated for lithographic evaluation under helium ion beam. Among all organic resists, particularly polymers such as poly(methyl methacrylate) (PMMA) are basic materials which show excellent sensitivity. Though they require a low dose, they suffer from pattern collapse.[18] At a high aspect ratio, these resists will have less mechanical strength and tend to collapse. In this context, the materials with requisite characteristics have to be designed and applied.[18]

5.1.1. Poly(methyl methacrylate). PMMA is an example of organic material that acts as a positive tone resist. Basically, this kind of long-chain polymer undergoes chain scission upon exposure to the beam of charged particles. The polymer breaks into smaller fragments with low molecular weight which possess more solubility than the long-chain polymer in a developer. As the exposed region dissolves in the developer and the remaining polymer stays as a structure, positive patterns are developed. In the past many years, PMMA has been used as one of the efficient primary resist materials for HIBL due to its adhesion capability over silicon substrates and low cost. In the late 1970s, PMMA with an average molecular weight of 1.85×10^5 g/mol was patterned to 2.7 μm feature size with a helium ion dose ~ 17 μC/cm^2.[40] The ion beam interactions with polymer resist include electronic and nuclear collisions. These two components act differently and lead to different chemical modifications and energy depositions. Further, the energy deposition rate also depends on the penetration depth as shown in Figure 5.[40]

Shi et al. explored the patterning performance of PMMA 495 K (4.95×10^5 g/mol) with EBL and HIBL.[29] The dose−response curve from the large area of resist film reveals that the PMMA behaves as a positive tone first and negative tone with increasing dose. Nevertheless, PMMA is highly sensitive to HIB compared to e-beam. The observed HIBL dose is ~2 μC/cm^2, while EBL showed more or less 60 times less sensitivity with a dose of ~120 μC/cm^2 (Figure 6).[41] Later, the difference in the proximity effect between HIBL and EBL was studied using the doughnut method described by Stevens et al.[42]

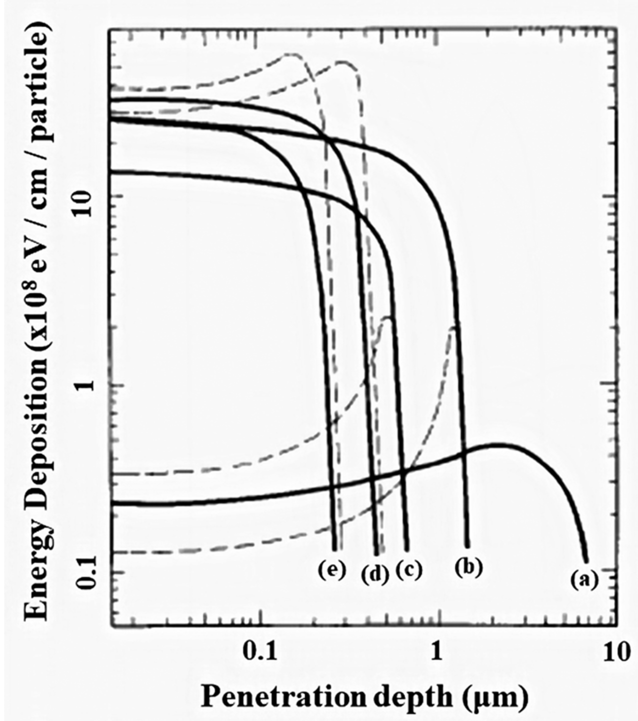

Figure 5. Calculated curves of energy deposition rate in PMMA resist as a function of the penetration depth: (a) 20 kV electron, (b) 200 kV He^+, (c) 60 kV He^+, (d) 250 kV Ar^+, and (e) 150 kV Ar^+. For the curves of the ions, solid and broken lines are of electronic and nuclear collision loss, respectively. Reprinted with permission from ref 40. Copyright 1979 IOP Publishing Ltd. (to improve image resolution, the x-axis and y-axis labels are rewritten).

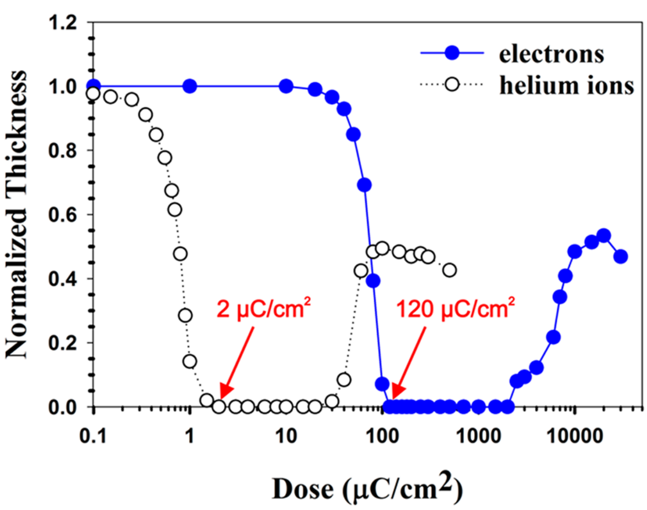

Figure 6. Comparison of the dose−response curves for 20 nm thick poly(methyl methacrylate) in electron beam lithography and helium ion beam lithography (HIBL). The measured sensitivities of 120 and 2 μC/cm^2 reveal a 60-fold improvement with HIBL. Reprinted with permission from ref 41. Copyright 2017 SPIE.

From the Gaussian approximation of the proximity equation, the range of backscattered ions/electrons was determined to be 67.1 nm and 3.26 μm for HIBL and EBL, respectively.[29] This suggests that HIBL is capable of producing high-density patterns with 50 times less proximity effect. This reduction in proximity effect supports the patterning of high-resolution dense patterns with an average critical dimension of 11.5 nm.[29]

At an increased exposure dose, PMMA acts as a negative tone resist. This could be due to cross-linking between the fragments at high concentrations. As the bond scissions happen to increase, then there are chances for coupling reactions to form a macromolecular network. The sensitivity dose observed for the negative tone patterning with PMMA is 68 μC/cm^2.[30]

5.1.2. Allotropes of Carbon. Carbon allotropes, viz., graphene and fullerene, are potential sources for the micro-/nanoelectronic devices.[43−48] Graphene is a two-dimensionally arranged carbon crystal and shows high stability. A suspended graphene nanodevice was fabricated by etching the graphene using a helium ion beam to a minimum feature size of ∼10 nm.[49] Afterward, graphene nanoribbon (GNR) arrays were fabricated with a width down to 5 nm half-pitch by Abbas et al.[50] Figure 7 shows the helium ion microscope (HIM) images of various graphene nanoribbon half-pitch patterns. The graphene nanoribbon (GNR) arrays with controlled width, space, and alignment were obtained. This patterned graphene device was then utilized as NO_2 gas sensor.[50]

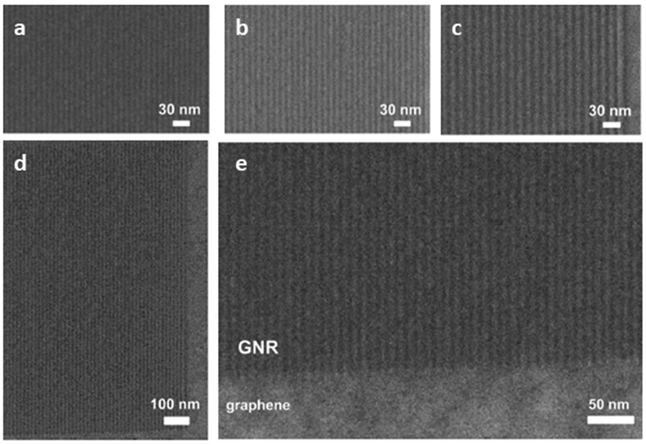

Figure 7. (a−c) Helium ion microscope images of (a) 5, (b) 6, and (c) 7.5 nm half-pitch arrays. (d) Helium ion microscope image of high aspect ratio GNRs (width × length is 5 nm × 1200 nm). (e) Helium ion microscope image shows a smooth interface between graphene and patterned GNRs. For all images, bright lines represent graphene. Reprinted with permission from ref 50. Copyright 2014 American Chemical Society.

In addition to graphene, fullerene-based molecular resists also were explored as potential materials for application toward HIBL.[51] These fullerene-based materials show the low molecular size, and thus they appeared to be potential for high-resolution patterning. The derivatives of fullerene act as a negative tone molecular resist in which the fragmentation of fullerene cage and subsequent cross-linking give an insoluble residue. As shown in Figure 8, derivatives of fullerene consist of functional groups on the surface of the cage which undergo chemical changes upon exposure with a beam of radiation. The high-resolution isolated line features were attained by EBL on chemically amplified fullerene derivatives with a line width of 13.6 nm.[52] The nonchemically amplified fullerene resists can have high etch resistance due to their high carbon content (more than known commercial resist SAL601 and close to eight times more than that of silicon under plasma etching).[51,53] Therefore, the fullerene-based resists are considered as potential resists for NGL.[51] But they are less sensitive under EBL compared to commercial resists. Although better resolutions were achieved with n-CARs using EBL, they were found to

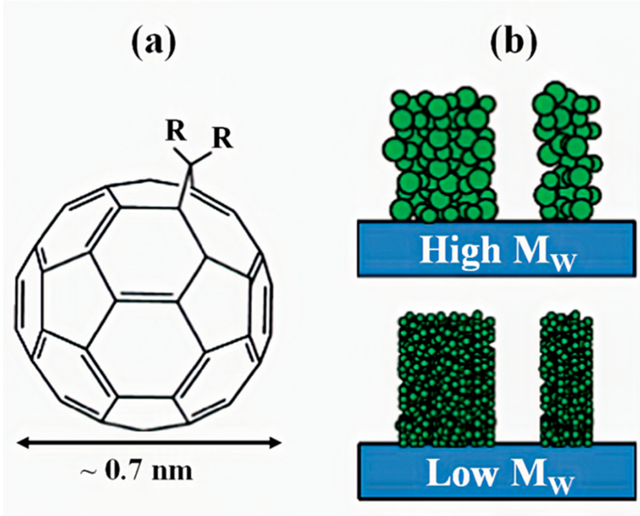

Figure 8. (a) Molecular diagram of generic fullerene resists. R represents the attached side chains to the C_{60} molecule. (b) Schematic showing the comparison between patterns formed from a high molecular weight resist and those from a low molecular weight resist after development. Reprinted with permission from ref 51. Copyright 2016 Elsevier B.V.

be relatively less sensitive.[51] The fullerenes with a smaller molecular size ∼ 0.7 nm and molecular weight (M_w) ∼ 1000 offer excessive potential to expand lithographic resolution with a reduced LER (Figure 8b). Since the molecular size and weight are less, the molecules on the edge of a line will not create much roughness. Hence the LER values are minimized with these parameters. In this context, a methanofullerene derivative of C_{60} was explored for HIBL fabrication. The large area of fullerene derivative exposed with ∼40 μC/cm^2 with a 30 keV helium ion beam resulted in 7.3 nm line features.[51] The same resist has been demonstrated to pattern 8.5 nm half-pitched lines with good feature separation.[51]

5.2. Inorganic Resists. Unlike organic resist materials, inorganic resists exhibit improved properties such as high contrast and enhanced etch resistance.[18] However, inorganic resists are disadvantageous because of their low sensitivity. The chemical structure of inorganic material is very stable, and this makes it hard to respond for radiation, but on the other hand, it restricts the pattern collapse. Hence the selection of resist for a particular application is important.[12,18]

5.2.1. Hydrogen Silsesquioxane. Hydrogen silsesquioxane (HSQ) is an example of inorganic resist material and a good example of a high-resolution negative tone resist. HSQ resist consists of Si−H bonds,[54] which undergo bond-breaking under the influence of beam of radiation, and Si centers cross-link to form a less soluble/insoluble inorganic matter. The bond energy of Si−H is ∼3 eV, which can be affected by the secondary electrons generated during the exposure. In this context, HSQ is a benchmark negative tone resist for the e-beam and EUV lithographic applications.[30,55−57] The critical dimensions of the patterns have reached down to sub-10 nm. Sidorkin et al. explored the patterning potential of HSQ toward scanning helium ion beam lithography (SHIBL).[58] Isolated dot patterns were attained in 5 and 55 nm thick HSQ films at a pitch of 98 nm. The diameters of the dot patterns are ∼6 and ∼14 nm for 5 and 55 nm thick films, respectively (Figure 9). These results demonstrate that HSQ is sensitive to the helium ion beam with a dose of 31 ± 3 μC/cm^2. This dose is nearly 4.4 times less in contrast with EBL dose. This concludes that this HSQ material under HIB shows high resolution with superior low proximity effect.[58]

Winston and co-workers found that sub-10 nm half-pitch patterning is feasible with HSQ resist. The 20 and 10 nm nested-"L" structures were fabricated in HSQ thin films with a line dose of 0.0834 nC/cm.[17] These patterns were developed in an aqueous salt

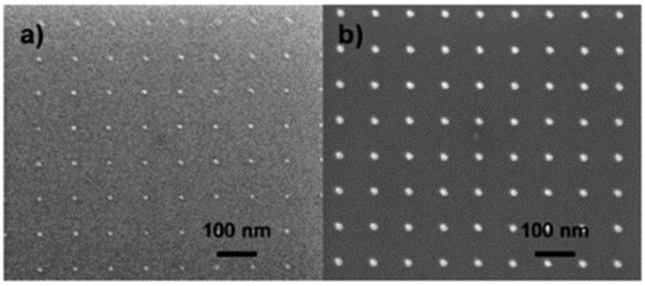

Figure 9. SEM images of arrays of dots written in (a) 5 and (b) 55 nm thick HSQ layers at 98 nm pitch using scanning helium ion beam lithography. Field of view is 900 nm in SE mode at 20 kV. Average dot diameters: (a) 6 ± 1 and (b) 14 ± 1 nm. Reprinted with permission from ref 58. Copyright 2009 American Vacuum Society.

developer (1% NaOH, 4% NaCl solution (w/v)). Later, the line pattern dimensions have been extended to single digit nanometer by Li et al.[26] Here they have fabricated a series of nested-L patterns with scanning focused helium ion beam by combination with nano-imprinting procedure. As shown in Figure 10, the 4 nm half-pitch features are patterned with a considerable resolution, while 3.5 nm HP patterns are not completely resolved.[26] This method has been useful to reuse the master molds to reproduce the structures which decrease the cost and improve the throughput.[19]

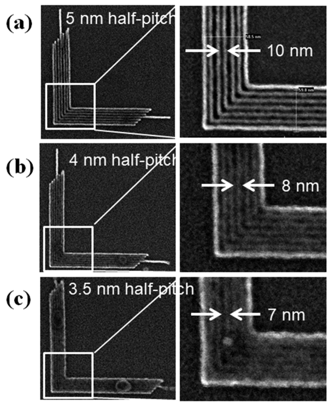

Figure 10. SEM images of (a) 5, (b) 4, and (c) 3.5 nm half-pitch nested-L's formed by helium ion beam lithography in an HSQ layer that was subsequently developed to remove the unexposed resist. Half-pitch patterns of 5 and 4 nm were clearly resolved. Although the 3.5 nm half-pitch patterns were not completely resolved, there were regions in which individual lines are distinct. Reprinted with permission from ref 26. Copyright 2012 American Vacuum Society.

The HSQ thin films were etched under neon and helium ion focused beam. Both beams exhibited the etching, but the etching rate slows with the helium ion beam. Nevertheless, helium ion focused beam can selectively eliminate the residual particles from the HSQ patterns.[59]

Sensitivity and contrast comparisons between EBL and HIBL with PMMA and HSQ resists are tabulated in Table 1. Irrespective of the type of material, HIBL shows superior sensitivity compared to EBL, whereas the contrasts are more or less equal with both tools.[30]

5.2.2. Hafnium-Based Resists. Hafnium sulfate is an inorganic compound and was reported to be an excellent source for the negative tone patterning under electron beam and UV photon exposure. This compound acquires the resist capability after adding a radiation-sensitive species, hydrogen peroxide (H_2O_2), to it.[60] HafSOx forms small clusters which are considered as building blocks of this inorganic resist.[61,62] This effective particle size allows the patterning with high resolution and low LER. Luo et al. carried out the lithographic performance of HafSOx by exposing it to He^+ ion and electron beam.[63] The results showed the line patterns below 10 nm (Figure 11) and the turn-on-dose, D_{100} (the dose at which the developed features start to have 100% of as-deposited resist thickness), was determined to be ∼4 $\mu C/cm^2$. This dose of HIBL is far better compared to the dose of EBL (∼420 $\mu C/cm^2$); it shows nearly 100-fold higher sensitivity. Moreover, D_{50} effectively reached ∼1 $\mu C/cm^2$ which matches with the sensitivity of chemically amplified resist (CAR) (0.93 $\mu C/cm^2$).[63]

Table 1. Sensitivity and Contrast for HSQ and PMMA 950*k* for He^+ and Electron Exposures at 30 keV[a] (Reused with Permission from Reference 30. Copyright 2012 Springer Nature)

resist	HSQ		PMMA-pos.		PMMA-neg.	
beam	e^-	He^+	e^-	He^+	e^-	He^+
sensitivity ($\mu C/cm^2$)	94	1.7	138	2	7891	68
contrast	2	2.3	4.2	3.7	3.9	4.7
enhancement	–	55	–	69	–	116

[a] The accuracies of dose and contrast are 2% and ±0.5, respectively.

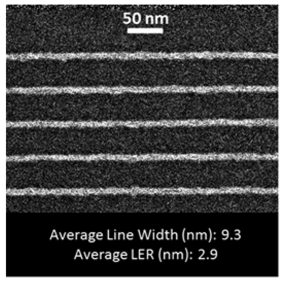

Figure 11. Line patterns showing below 10 nm average line width and LER (3σ) 2.9 nm. Reprinted with permission from ref 63. Copyright 2016 SPIE.

5.2.3. Alumina-Based Resist. Cattoni et al. have achieved sub-10 nm features with alumina-based resist material by HIBL.[64] Previously, Brusantin and co-workers developed this hybrid organic−inorganic resist and investigated its EBL performance.[65] This resist is synthesized by sol−gel synthetic method and forms inorganic alumina upon exposure to the beam of electron or photon. Consequently, the radiation exposure results in chemical changes in the organic part of the material leading to solubility switch. Therefore, FHIB has been used to pattern 5 nm isolated lines and dense line patterns with 20 nm pitch.[64] Various isolated pitches and pitches of 64, 40, and 20 nm were demonstrated with the 30 keV FHIB, dose ranging from 200 to 700 $\mu C/cm^2$ (Figure 12). The observations found results superior to those of EBL, due to less proximity effect. Further, the resolution, LER, and selectivity were substantially improved. However, the limitations associated with this alumina resist are in terms of stability, the time window of the process, and resist solution lifetime. But these variables can be addressed by optimizing other parameters such as postapplication bake (PAB), postexposure bake (PEB), and developer concentration, etc.[64]

5.2.4. Change in Electronic and Optical Properties of MoS_2 by HIB. Helium ion beam is able to change the crystal structure, which in turn may modify the electronic and optical properties of some of the materials, such as MoS_2.[66−68] This has been realized since helium ion effectively interacts with the material and brings in various changes including structural changes, compositional changes, geometrical changes, and material properties. Therefore, amorphous MoS_2 nanostructures with metallic behavior were fabricated.[69] The structures with 7 nm dimensions and minimized edge damage (∼1 nm) were achieved successfully (Figure 13). Along with MoS_2, other materials were also investigated such as Mn_2O_3 and TiO_2, and their corresponding nanoribbons were created by He^+ milling.[69]

https://dx.doi.org/10.1021/acsaelm.0c00627
ACS Appl. Electron. Mater. XXXX, XXX, XXX−XXX

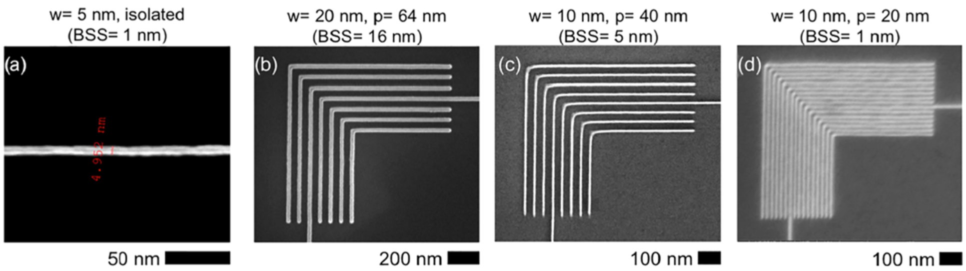

Figure 12. SEM images of FHIB exposed alumina resist (20 nm thick). (a) 5 nm isolated line exposed with BSS = 1 nm. (b) 20 nm lines exposed with BSS = 16 nm and p = 64 nm. (c) 10 nm lines exposed with BSS = 5 nm and p = 40 nm. (d) 10 nm lines exposed with BSS = 1 nm and p = 20 nm. Reprinted with the permission from ref 64. Copyright 2018 Elsevier.

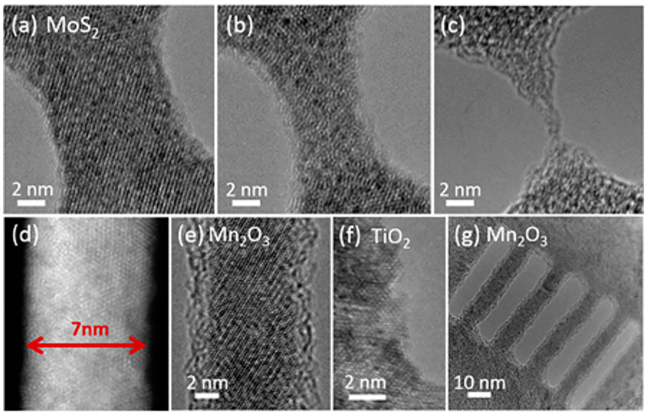

Figure 13. He^+ fabricated freestanding nanoribbons in 2D materials. (a) TEM image of a 9 nm wide crystalline MoS_2 nanoribbon. (b) 5 nm wide amorphous MoS_2 nanoribbon. (c) Amorphous nanoribbon with a minimum width of less than 1 nm. (d) STEM image of a 7 nm wide crystalline MoS_2 nanoribbon. (e) 9 nm wide crystalline Mn_2O_3 nanoribbon milled with HIM. (f) TiO_2 edge milled with HIM. (g) Array of 10 nm wide Mn_2O_3 nanoribbons milled with HIM. Reprinted with permission from ref 69. Copyright 2015 American Chemical Society.

Recently, rhombus-shaped nanopores were created in MoS_2 monolayers using He^+ beam.[70] In this work, the effect of He^+ dose on the shape and size of the nanopore has been investigated. At lower, medium, and high doses corresponding elliptical-, rhombus-, and polygon-shaped nanopores were observed, respectively (Figure 14).

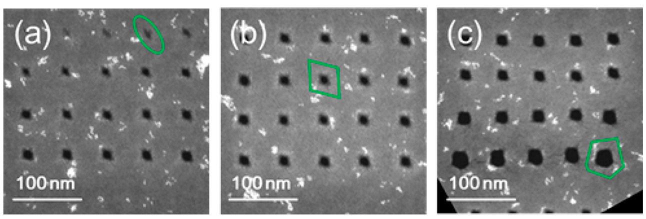

Figure 14. Scanning transmission electron microscopy−high-angle annular dark field (STEM-HAADF) images of nanopores to show the evolution of nanopore shapes as the dose increases. The beam is modulated to be elliptical. (a) STEM-HAADF image of nanopores drilled at low dose (2.17×10^{-5} to 4.34×10^{-4} nC). The elliptical nanopore is guided by an elliptical frame. (b) STEM-HAADF image of nanopores drilled at a medium dose (($4.557-8.68) \times 10^{-4}$ nC). Rhombus-shaped nanopore is guided by a rhombus frame. (c) STEM-HAADF images of nanopores drilled at a large dose (8.897×10^{-4} to 2.17×10^{-3} nC). The polygon-shaped nanopore is guided by a polygon frame. Reprinted with permission from ref 70. Copyright 2020 IOP Publishing Ltd.

5.3. Chemically Amplified Resists. Many chemically amplified resist substances are being used for nanofabrication using different lithography techniques including DUVL, EUVL, EBL, and so on. Likewise, CARs can also have the potential toward nanofeature fabrication by ion beam lithography. The chemically amplified resist composition generally contains a polymer bearing acid labile group and a photoacid generator (PAG) as the key components. The acid labile group is responsible for polarity switching when it is deprotected upon chemical reaction with acid. The lithographic mechanism using CARs involves the presence of a photoacid generator (PAG).[32] This PAG generates the strong acid functionalities during the exposure, and these will initiate and catalyze the chemical reactions during postexposure bake. Thus, the sensitivity may be enhanced. But there are some factors that affect the high resolution of the patterns. Acid diffusion is one among them; if the diffusion of acid is non-uniform in the resist thin layer, then it leads to creation of uneven modifications. Due to acid diffusion, the roughness at the edges of the lines arises.[32] However, it can be avoided by incorporating the PAG in the backbone of the resist,[32] though conventional CARs are highly sensitive toward radiation but they often have less etch resistance.[12] The acid generation can also be triggered by helium ion beam which subsequently leads to formation of a pattern after PEB and development. In this context, the HIBL LER efficiencies of various CAR substances were examined by Eder-Kapl et al. They assessed the competence among Shipley UVIIHS, Shipley F, Infineon experimental CAR no. 1 and Infineon experimental CAR no. 2 (Table 2).[31]

5.4. Organic−Inorganic Hybrid Resists. In addition to CARs, nonchemically amplified resists (n-CAR) have also been considered for HIBL application. Currently, many novel hybrid organic−inorganic n-CARs are developed for this purpose. The synergistic interactions between organic and inorganic units can lead to enhance the properties such as sensitivity, adhesion, resolution, and etch resistance as compared to pure organic resist films.[71−73] In this perspective, a new n-CAR MAPDSA-*co*-MAPDST (Figure 15) was developed by our group for sub-20 nm patterning studies using HIBL technique.[74] This has been reported as the first helium ion active hybrid resist. Here MAPDSA [(4-(methacryloyloxy)phenyl dimethylsulfoniumhexaflouroantimonate)] is an inorganic antimony containing monomer, whereas MAPDST [(4-(methacryloyloxy)phenyl) dimethylsulfonium trifluoromethanesulfonate] is a radiation-sensitive organic moiety that can undergo chemical transformations to create polarity differences. The hybrid copolymer resist MAPDSA-MAPDST was synthesized by copolymerization of two units. The 2.15%-MAPDSA-MAPDST resist was used to pattern 20 nm (L/4S) features at a dose of 60 $\mu C/cm^2$ with ultralow sensitivity (7.2 $\mu C/cm^2$) and LER (1.27 ± 0.31 nm) as shown in the Figure 16. These LER values were found to be better than the earlier reported HIBL resist materials.[74]

Later, we developed another hybrid organic−inorganic n-CAR, i.e., MAPDST-*co*-ADSM (ADSM = (acetyldibutylstannyl methacrylate)) for nanopatterning by HIBL.[75] As depicted in Figure 17, the inorganic ADSM is a tin containing compound and acts as a sensitizer. This MAPDST-*co*-ADSM resist with 2 wt % ADSM showed sub-15 nm negative tone patterns at a dose of ~50 $\mu C/cm^2$. These patterns

https://dx.doi.org/10.1021/acsaelm.0c00627
ACS Appl. Electron. Mater. XXXX, XXX, XXX−XXX

Table 2. Resists and Processing Parameters Used for the Experiment (Reused with Permission from Reference 31. Copyright 2004 Elsevier)

resist	Shipley UVIIHS	Shipley F	Infineon CAR no. 1		Infineon CAR no. 2	
resist thickness	290 nm	150 nm	150 nm		180 nm	
prebake	130 °C/60s	130 °C/60s	140 °C/60s		140 °C/60s	
post exposure bake	130 °C/90s	130 °C/90s	140 °C/60s	30 °C/60s	140 °C/60s	
development	20 s LDD26W	45 s LDD26W	30 s, 2:1 H_2O:TMAH		60 s, 2:1 H_2O:TMAH	30 s, TMAH (pure)
dose to clear large areas	0.2 $\mu C/cm^2$	1.4 $\mu C/cm^2$	0.9 $\mu C/cm^2$	1.0 $\mu C/cm^2$	1.8 $\mu C/cm^2$	0.7 $\mu C/cm^2$
remarks	high sensitivity	similar to UVIIHS with unknown additives	methacrylic acid copolymer with suitable PAG[a] and base		similar to Infineon CAR no. 1 but with reduced solvent for thicker resist layers	

[a]PAG = photoacid generator.

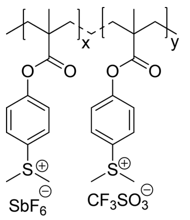

Figure 15. Chemical structures of the 2.15%-MAPDSA-MAPDST copolymer resist. Reprinted with permission from ref 74. Copyright 2017 SPIE.

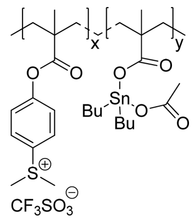

Figure 17. Chemical structure of MAPDST-*co*-ADSM copolymer resist for HIBL studies. Reprinted with permission from ref 75. Copyright 2018 SPIE.

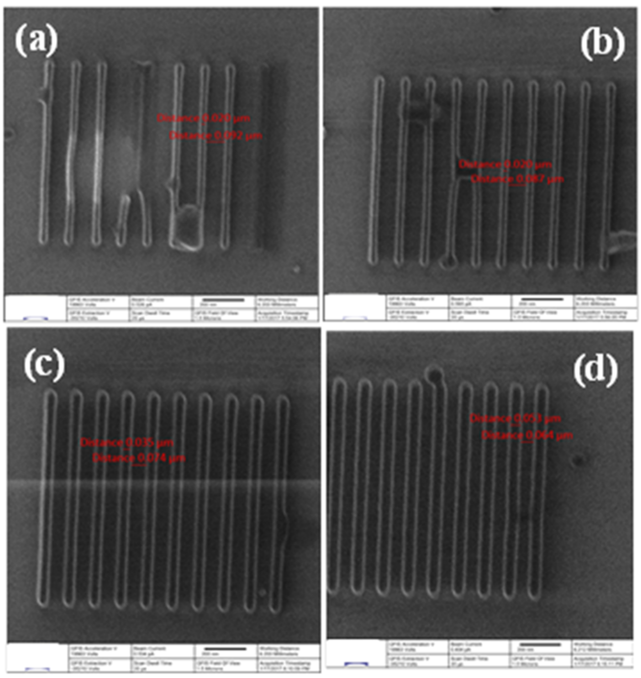

Figure 16. Line features of 20 nm (L/4S) of the 2.15%-MAPDSA-MAPDST resist at various doses: (a) 50, (b) 60, (c) 340, and (d) 540 $\mu C/cm^2$. Reprinted with permission from ref 74. Copyright 2017 SPIE.

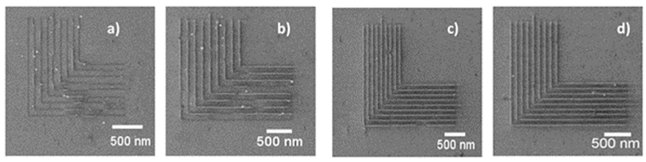

Figure 18. Dose test analysis of single pixel line patterns of the L-shaped features obtained from the MAPDST-*co*-ADSM resist at various doses (a) 30, (b) 40, (c) 50, and (d) 100 pC/cm. Reprinted with permission from ref 75. Copyright 2018 SPIE.

exhibited clear LER and LWR values as ∼1.67 ± 0.27 nm and ∼2.20 nm respectively. Then, the single-pixel exposure led to producing the line pattern of 10 nm with a dose of ∼50.48 pC/cm (Figure 18).[75] The inorganic tin sensitizer was probably responsible for the better resolution. In addition to experimental details, Monte Carlo (MC) ion trajectory simulations were carried out to elucidate the sample damage and the energy transfer efficiency.

Recently, metal−organic clusters (MOCs) have attained considerable attention largely due to their narrow size distribution and uniform thin film formation potential.[76−78] Since these factors influence the resolution and sensitivity of the material, Kumar et al. have developed a negative tone nickel-based, metal−organic cluster (Ni-MOC) for HIBL application (Figure 19).[79] This MOC cluster

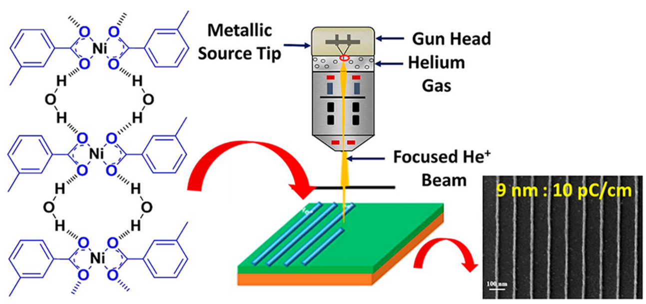

Figure 19. Nickel metal−organic clusters have been designed for next-generation lithography and patterning of sub-10 nm features using HIBL. Reprinted with permission from ref 79. Copyright 2020 American Chemical Society.

consists of a nickel core covalently linked with an organic ligand, *m*-toulic acid, to form a building block with an average cluster diameter of 2 nm. These synthesized Ni-MOCs showed well-resolved ∼9 nm line patterns at a sensitivity of 22 $\mu C/cm^2$. Furthermore, low LER and LWR were achieved as 1.81 ± 0.06 nm and 2.90 ± 0.06 nm, respectively.[79]

Lewis et al. have developed a chromium-based negative tone metal−organic resist for the application toward the fabrication of field emission transistor.[76,80] The structure of the resist is shown in Figure

20 and consists of eight chromium atoms bound in a ring-like structure. The exterior portion of this ring is composed of 16 units of

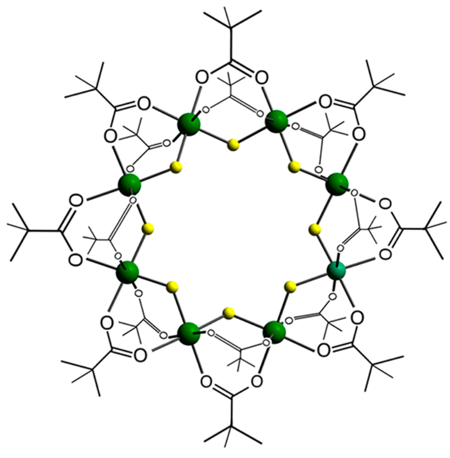

Figure 20. Structure of the $Cr_8F_8(pivalate)_{16}$ molecule in a ball-and-stick representation. Chromium atoms are green, and fluorine atoms are yellow. Hydrogen atoms are omitted for clarity. Reprinted with permission from ref 76. Copyright 2019 American Chemical Society.

tert-butyl groups (pivalates), and these pivalate groups help in the solubility of the resist in nonpolar solvents. Therefore, the chemical formula of this resist is denoted as $Cr_8F_8(O_2C^tBu)_{16}$ or $Cr_8F_8(pivalate)_{16}$. This resist showed the capability to produce sub-10 nm structures on silicon and tungsten by HIBL. The HIBL dose to fabricate the 5 nm wide, continuous lines on 16 nm pitches is 22 pC/cm. Figure 21 represents various sizes of features and their

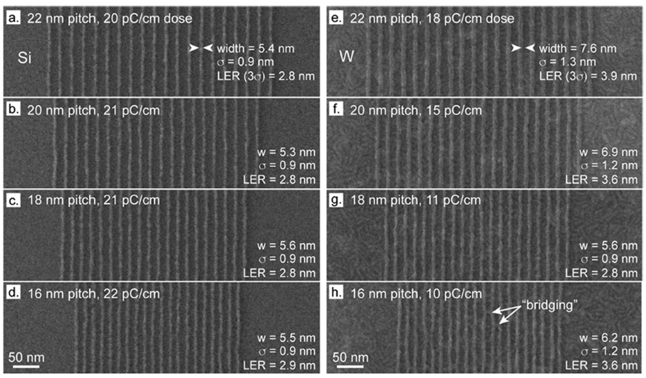

Figure 21. Plan-view HIM images of lines spaced with pitches of 22, 20, 18, and 16 nm on silicon substrate (a−d, respectively) and on a 100 nm thick tungsten film that was sputter-deposited onto a silicon substrate (e−h, respectively). Average width (w), standard deviation (σ), and line-edge roughness (LER) (3σ) to the nearest 0.1 nm were determined using GenISys ProSEM software. Reprinted with permission from ref 76. Copyright 2019 American Chemical Society.

corresponding dosages on silicon and tungsten substrates. After exposure, this metal−organic resist undergoes chemical changes to produce a chromium oxide based material which will exhibit high etch resistance.[76]

5.5. Nanoparticles. In recent time, metal nanoparticles (NPs) have gained significant importance in the field of semiconductor and electronics industries. Different properties associated with the metal NPs lead to varying electronic band gap and photoabsorption enhancement.[81] Particularly, some of the metal NPs show high-absorption cross-section due to their high optical density (O.D.). Such characteristic properties of those nanoparticles, result in producing the plasmons by absorbed photon from the NPs, called plasmonic effect. These plasmons cause photomultiplication, in which plasmons effectively interact with the proximate regime in order to enhance the kinetics.[82] Profoundly, this photomultiplication can promote high-volume manufacturing (HVM) by next-generation lithography.[83] With the benefits supported by the plasmonic NPs, those can be used instead of PAG in polymers for the same custom. Sharma et al. designed a negative tone nanochemically amplified resist with silver nanoparticles embedded in MAPDST homopolymer (Figure 22).[84] The diameter of Ag NPs is ∼2 nm and showed O.D.

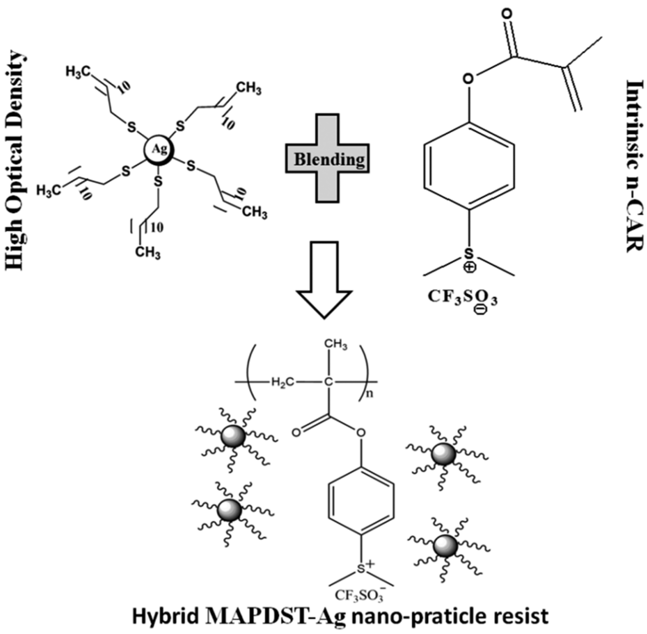

Figure 22. Schematic synthesis of MAPDST-Ag. Reprinted with permission from ref 84. Copyright 2020 SPIE.

12 with respect to carbon. This hybrid material was investigated under He^+ beam to fabricate ∼12 nm features with a sensitivity of 50.4 $\mu C/cm^2$ (Figure 23).[84]

6. CONCLUSION AND FUTURE PERSPECTIVE

In summary, HIBL is an emerging lithographic method to pattern sub-5 nm high-density features. Various developments in terms of technical aspects of the HIBL tool have been carried out to minimize the probe size down to sub-nanometer. The lighter and high-intensity helium ion beam is essential to

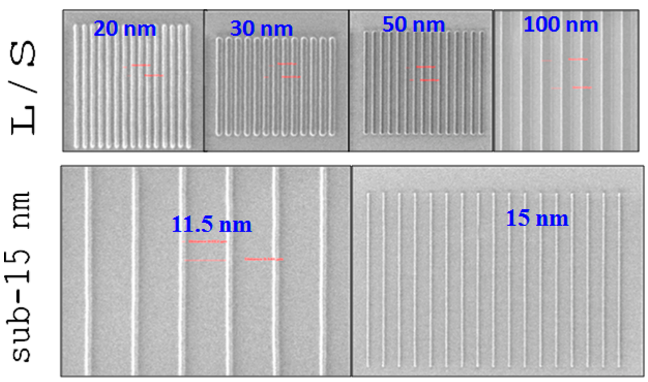

Figure 23. High-resolution patterning with HIBL; line/space patterns of 20, 30, 50, and 100 nm on MAPDST-Ag (top row). Isolated lines of 11.5 and 15 nm with ultralow LER (bottom row). Reprinted with permission from ref 84. Copyright 2020 SPIE.

https://dx.doi.org/10.1021/acsaelm.0c00627
ACS Appl. Electron. Mater. XXXX, XXX, XXX−XXX

decreasing the backscattering and also to producing a large number of secondary electrons. These particular features make He^+ as a prominent source to reduce the proximity effects. Moreover, this property helps in enhancing the resolution and sensitivity of the particular resist material with respect to the electron beam. Though the ion beam affects the target sample during exposure, it can be overcome by optimizing the dose. Given the advantages of HIBL, several resist materials were designed, developed, and investigated under He^+ beam to generate the patterns. The quite known organic polymer, PMMA, has been investigated to act as a positive as well as negative tone resist under He^+ beam. At lower doses, it acts as a positive tone resist, but at higher dose it behaves as a negative tone resist. Other organics such as carbon allotropes also were successfully established to have potential as resists for HIBL technology. In addition to organics, various inorganic materials such as HSQ, HfSOx, alumina, and MoS_2, etc., have been explored to be negative tone thin film resists for HIBL. Further, organic–inorganic hybrid resists were utilized to improve the sensitivity of the material. Also, these hybrid resists possess good etch resistance which in turn lower the sample damage. Later, the possibility of using plasmonic metal nanoparticles embedded into the resist matrix to improve the sensitivity by the photomultiplication process was successfully explored and established. Irrespective of the type of the material, HIBL is a promising candidate for patterning because of the practically negligible BEs from the resist–substrate interaction, which potentially make it ideal for both a confined and highly dense feature, and it performed superior to electron beam in most occasions. But it is limited by throughput and large-scale patterning as it is a serial-writing technique. However, given its potential in patterning sub-5 nm features, and considering this technology as an emerging nanopatterning lithography technique, a large scope for a new and efficient resist platform still remains there as the number of resists for HIBL are quite limited in the literature.

AUTHOR INFORMATION

Corresponding Authors

Subrata Ghosh – *School of Basic Sciences (SBS), Indian Institute of Technology (IIT), Mandi, Himachal Pradesh 175005, India*; orcid.org/0000-0002-8030-4519; Email: subrata@iitmandi.ac.in

Kenneth E. Gonsalves – *School of Basic Sciences (SBS), Indian Institute of Technology (IIT), Mandi, Himachal Pradesh 175005, India*; Email: kenneth@iitmandi.ac.in

Authors

Nagarjuna Ravi Kiran – *School of Basic Sciences (SBS), Indian Institute of Technology (IIT), Mandi, Himachal Pradesh 175005, India*

Manvendra Chauhan – *School of Computing and Electrical Engineering (SCEE), Indian Institute of Technology (IIT), Mandi, Himachal Pradesh 175005, India*

Satinder K. Sharma – *School of Computing and Electrical Engineering (SCEE), Indian Institute of Technology (IIT), Mandi, Himachal Pradesh 175005, India*; orcid.org/0000-0001-9313-5550

Complete contact information is available at: https://pubs.acs.org/10.1021/acsaelm.0c00627

Notes

The authors declare no competing financial interest.

ACKNOWLEDGMENTS

Financial support from Uchchyatar Avishkar Yojona (UAY) (Grant No. IITMandi_005) is thankfully acknowledged.

REFERENCES

(1) Sanders, D. P. Advances in patterning materials for 193 nm immersion lithography. *Chem. Rev.* **2010**, *110*, 321–360.

(2) Wallraff, G.; Hinsberg, W. Lithographic imaging techniques for the formation of nanoscopic features. *Chem. Rev.* **1999**, *99*, 1801–1822.

(3) Tohge, N.; Ueno, R.; Chiba, F.; Kintaka, K.; Nishii, J. Characteristics of diffraction gratings fabricated by the two-beam interference method using photosensitive hybrid gel films. *J. Sol-Gel Sci. Technol.* **2000**, *19*, 119–123.

(4) Saifullah, M.; Subramanian, K.; Tapley, E.; Kang, D. J.; Welland, M.; Butler, M. Sub-10 nm electron beam nanolithography using spin-coatable TiO_2 resists. *Nano Lett.* **2003**, *3*, 1587–1591.

(5) Voicu, N. E.; Saifullah, M.; Subramanian, K.; Welland, M. E.; Steiner, U. TiO_2 patterning using electro-hydrodynamic lithography. *Soft Matter* **2007**, *3*, 554–557.

(6) Duoss, E. B.; Twardowski, M.; Lewis, J. A. Sol-gel inks for direct-write assembly of functional oxides. *Adv. Mater.* **2007**, *19*, 3485–3489.

(7) Sung, S.; Park, S.; Cha, S.; Lee, W. J.; Kim, C. H.; Yoon, M. H. Direct patterning of sol–gel metal oxide semiconductor and dielectric films via selective surface wetting. *RSC Adv.* **2015**, *5*, 38125–38129.

(8) Fu, L.; Liu, X.; Zhang, Y.; Dravid, V. P.; Mirkin, C. A. Nanopatterning of "hard" magnetic nanostructures via dip-pen nanolithography and a sol-based ink. *Nano Lett.* **2003**, *3*, 757–760.

(9) Lim, S. H.; Saifullah, M.; Hussain, H.; Loh, W. W.; Low, H. Y. Direct imprinting of high resolution TiO_2 nanostructures. *Nanotechnology* **2010**, *21*, 285303.

(10) Azimi, S.; Song, J.; Li, C.; Mathew, S.; Breese, M.; Venkatesan, T. Nanoscale lithography of $LaAlO_3/SrTiO_3$ wires using silicon stencil masks. *Nanotechnology* **2014**, *25*, 445301.

(11) Ali Mohammad, M.; Muhammad, M.; Dew, S. K.; Stepanova, M. In *Nanofabrication: Techniques and principles*; Stepanova, M., Dew, S. K., Eds.; Springer: Vienna, 2012; pp 11–41, DOI: 10.1007/978-3-7091-0424-8_2.

(12) Li, L.; Liu, X.; Pal, S.; Wang, S.; Ober, C. K.; Giannelis, E. P. Extreme ultraviolet resist materials for sub-7 nm patterning. *Chem. Soc. Rev.* **2017**, *46*, 4855–4866.

(13) Manouras, T.; Argitis, P. High sensitivity resists for EUV lithography: A review of material design strategies and performance results. *Nanomaterials* **2020**, *10*, 1593–1616.

(14) Yang, J. K.; Cord, B.; Duan, H.; Berggren, K. K.; Klingfus, J.; Nam, S. W.; Kim, K. B.; Rooks, M. J. Understanding of hydrogen silsesquioxane electron resist for sub-5-nm-half-pitch lithography. *J. Vac. Sci. Technol., B* **2009**, *27*, 2622–2627.

(15) Notte, J.; Ward, B.; Economou, N.; Hill, R.; Percival, R.; Farkas, L.; McVey, S.; et al. An introduction to the helium ion microscope. *AIP Conf. Proc.* **2007**, *931*, 489–496.

(16) Ward, B.; Notte, J. A.; Economou, N. Helium ion microscope: A new tool for nanoscale microscopy and metrology. *J. Vac. Sci. Technol., B* **2006**, *24*, 2871–2874.

(17) Winston, D.; Cord, B. M.; Ming, B.; Bell, D.; DiNatale, W.; Stern, L.; Vladar, A.; Postek, M.; Mondol, M.; Yang, J.; Berggren, K. K. Scanning-helium-ion-beam lithography with hydrogen silsesquioxane resist. *J. Vac. Sci. Technol., B* **2009**, *27*, 2702–2706.

(18) Luo, C.; Xu, C.; Lv, L.; Li, H.; Huang, X.; Liu, W. Review of recent advances in inorganic photoresists. *RSC Adv.* **2020**, *10*, 8385–8395.

(19) Shi, X.; Boden, S. A. Scanning helium ion beam lithography. *Front. Nanosci.* **2016**, *11*, 563–594.

(20) Watt, F.; Bettiol, A.; Van Kan, J.; Teo, E.; Breese, M. Ion beam lithography and nanofabrication: A review. *Int. J. Nanosci.* **2005**, *4*, 269–286.

(21) McCord, M. A.; Rooks, M. J. *Handbook of microlithography, micromachining and microfabrication*; SPIE Press, **1997**, pp 136−249.
(22) Joshi-Imre, A.; Bauerdick, S. Direct-write ion beam lithography. *J. Nanotechnol.* **2014**, *2014*, No. 170415.
(23) Scipioni, L.; Sanford, C. A.; Notte, J.; Thompson, B.; McVey, S. Understanding imaging modes in the helium ion microscope. *J. Vac. Sci. Technol., B* **2009**, *27*, 3250−3255.
(24) Matsui, S.; Kojima, Y.; Ichiai, Y.; Honda, T. High-resolution focused ion beam lithography. *J. Vac. Sci. Technol., B: Microelectron. Process. Phenom.* **1991**, *9*, 2622−2632.
(25) Kubena, R.; Ward, J.; Stratton, F.; Joyce, R.; Atkinson, G. A low magnification focused ion beam system with 8 nm spot size. *J. Vac. Sci. Technol., B: Microelectron. Process. Phenom.* **1991**, *9*, 3079−3083.
(26) Li, W. D.; Wu, W.; Stanley Williams, R. Combined helium ion beam and nanoimprint lithography attains 4 nm half-pitch dense patterns. *J. Vac. Sci. Technol., B: Nanotechnol. Microelectron.: Mater., Process., Meas., Phenom.* **2012**, *30*, 06F304.
(27) Horiuchi, K.; Itakura, T.; Ishikawa, H. Fine pattern lithography using a helium field ion source. *J. Vac. Sci. Technol., B: Microelectron. Process. Phenom.* **1988**, *6*, 241−244.
(28) Hill, R.; Faridur Rahman, F. H. M. Advances in helium ion microscopy. *Nucl. Instrum. Methods Phys. Res., Sect. A* **2011**, *645*, 96−101.
(29) Shi, X.; Prewett, P.; Huq, E.; Bagnall, D.; Boden, S. A quantitative comparison between helium ion and electron beam lithography on PMMA resist. *42nd Intional Conference on Micro and Nano Engineering*, Vienna, Austria, Sep. 19−23, 2016.
(30) van der Drift, E.; Maas, D. J. Helium ion lithography. In *Nanofabrication: Techniques and Principles*; Stepanova, M., Dew, S., Eds.; Springer: Vienna, 2012; pp 93−116, DOI: 10.1007/978-3-7091-0424-8_4.
(31) Eder-Kapl, S.; Loeschner, H.; Zeininger, M.; Fallmann, W.; Kirch, O.; Patsis, G. P.; Constantoudis, V.; Gogolides, E. Line edge roughness investigation on chemically amplified resist materials with masked helium ion beam lithography. *Microelectron. Eng.* **2004**, *73-74*, 252−258.
(32) Gangnaik, A. S.; Georgiev, Y. M.; Holmes, J. D. New generation electron beam resists: a review. *Chem. Mater.* **2017**, *29*, 1898−1917.
(33) Postek, M. T.; Vladar, A.; Archie, C.; Ming, B. Review of current progress in nanometrology with the helium ion microscope. *Meas. Sci. Technol.* **2011**, *22*, 024004−024017.
(34) Hlawacek, G.; Veligura, V.; van Gastel, R.; Poelsema, B. Helium ion microscopy. *J. Vac. Sci. Technol., B: Nanotechnol. Microelectron.: Mater., Process., Meas., Phenom.* **2014**, *32*, 020801.
(35) Inai, K.; Ohya, K.; Ishitani, T. Simulation study on image contrast and spatial resolution in helium ion microscope. *J. Electron Microsc.* **2007**, *56*, 163−169.
(36) Hill, R.; Notte, J. A.; Scipioni, L. Scanning helium ion microscopy. *Adv. Imaging Electron Phys.* **2012**, *170*, 65−148.
(37) Alkemade, P. F.; Koster, E. M.; van Veldhoven, E.; Maas, D. J. Imaging and nanofabrication with the helium ion microscope of the van leeuwenhoek laboratory in delft. *Scanning* **2012**, *34*, 90−100.
(38) Livengood, R.; Tan, S.; Greenzweig, Y.; Notte, J.; McVey, S. Subsurface damage from helium ions as a function of dose, beam energy, and dose rate. *J. Vac. Sci. Technol., B* **2009**, *27*, 3244−3249.
(39) Livengood, R. H.; Grumski, M.; Greenzweig, Y.; Liang, T.; Jamison, R.; Xie, Q. Helium ion microscope invasiveness study and novel imaging analysis for semiconductor applications. *Phys. Procedia* **2008**, *1*, 143−148.
(40) Komuro, M.; Atoda, N.; Kawakatsu, H. Ion beam exposure of resist materials. *J. Electrochem. Soc.* **1979**, *126*, 483.
(41) Boden, S.; Shi, X. Helium ion beam lithography for sub-10 nm pattern definition. *SPIE Newsroom* **2017**, DOI: 10.1117/2.1201702.006839.
(42) Stevens, L.; Jonckheere, R.; Froyen, E.; Decoutere, S.; Lanneer, D. Determination of the proximity parameters in electron beam lithography using doughnut-structures. *Microelectron. Eng.* **1986**, *5*, 141−150.
(43) Novoselov, K.; Geim, A.; Morozov, S.; Jiang, D.; Zhang, Y.; Dubonos, S.; Grigorieva, I.; Firsov, A. Electric field effect in atomically thin carbon films. *Science* **2004**, *306*, 666−669.
(44) Novoselov, K. S.; Geim, A. The rise of graphene. *Nat. Mater.* **2007**, *6*, 183−191.
(45) Lemme, M. C.; Echtermeyer, T. J.; Baus, M.; Kurz, H. A graphene field-effect device. *IEEE Electron Device Lett.* **2007**, *28*, 282−284.
(46) Rao, A. M.; Zhou, P.; Wang, K.-A.; Hager, G. T.; Holden, J. M.; Wang, Y.; Lee, W.- T.; Bi, X.-X.; Eklund, P. C.; Cornett, D. S.; Duncan, M. A.; Amster, I. J. Photoinduced Polymerization of Solid C_{60} Films. *Science* **1993**, *259*, 955−957.
(47) Tada, T.; Kanayama, T. Nanolithography using fullerene films as an electron beam resist. *J. Photopolym. Sci. Technol.* **1997**, *10*, 647−650.
(48) Chen, X.; Palmer, R.; Robinson, A. A high resolution water soluble fullerene molecular resist for electron beam lithography. *Nanotechnology* **2008**, *19*, 275308.
(49) Lemme, M. C.; Bell, D. C.; Williams, J. R.; Stern, L. A.; Baugher, B. W.; Jarillo-Herrero, P.; Marcus, C. M. Etching of graphene devices with a helium ion beam. *ACS Nano* **2009**, *3*, 2674−2676.
(50) Abbas, A. N.; Liu, G.; Liu, B.; Zhang, L.; Liu, H.; Ohlberg, D.; Wu, W.; Zhou, C. Patterning, characterization, and chemical sensing applications of graphene nanoribbon arrays down to 5 nm using helium ion beam lithography. *ACS Nano* **2014**, *8*, 1538−1546.
(51) Shi, X.; Prewett, P.; Huq, E.; Bagnall, D. M.; Robinson, A. P.; Boden, S. A. Helium ion beam lithography on fullerene molecular resists for sub-10 nm patterning. *Microelectron. Eng.* **2016**, *155*, 74−78.
(52) Yang, D.; Frommhold, A.; Xue, X.; Palmer, R.; Robinson, A. Chemically amplified phenolic fullerene electron beam resist. *J. Mater. Chem. C* **2014**, *2*, 1505−1512.
(53) Manyam, J.; Manickam, M.; Preece, J.; Palmer, R.; Robinson, A. Plasma etching of high-resolution features in a fullerene molecular resist. *Proceedings, Advances in Resist Materials and Processing Technology XXVIII, International Society for Optics and Photonics*; SPIE, 2011; Vol. *7972*, 79722−79733, DOI: 10.1117/12.879469.
(54) Namatsu, H.; Yamaguchi, T.; Nagase, M.; Yamazaki, K.; Kurihara, K. Nano-patterning of a hydrogen silsesquioxane resist with reduced linewidth fluctuations. *Microelectron. Eng.* **1998**, *41*, 331−334.
(55) Grigorescu, A. E.; Van der Krogt, M. C.; Hagen, C. W.; Kruit, P. Influence of the development process on ultimate resolution electron beam lithography, using ultrathin hydrogen silsesquioxane resist layers. *J. Vac. Sci. Technol., B* **2007**, *25*, 1998−2003.
(56) Fan, D.; Ekinci, Y. Photolithography reaches 6 nm half-pitch using EUV light. *J. Micro/Nanolithogr., MEMS, MOEMS* **2016**, *15*, 033505.
(57) Mojarad, N.; Hojeij, M.; Wang, L.; Gobrecht, J.; Ekinci, Y. Single-digit-resolution nanopatterning with extreme ultraviolet light for the 2.5 nm technology node and beyond. *Nanoscale* **2015**, *7*, 4031−4037.
(58) Sidorkin, V.; Van Veldhoven, E.; Van der Drift, E.; Alkemade, P.; Salemink, H.; Maas, D. Sub-10-nm nanolithography with a scanning helium beam. *J. Vac. Sci. Technol., B* **2009**, *27*, L18−L20.
(59) Xia, D.; Zhu, X.; Khanom, F.; Runt, D. Neon and helium focused ion beam etching of resist patterns. *Nanotechnology* **2020**, *31*, 475301−475311.
(60) Oleksak, R. P.; Ruther, R. E.; Luo, F.; Fairley, K. C.; Decker, S. R.; Stickle, W. F.; Johnson, D. W.; Garfunkel, E. L.; Herman, G. S.; Keszler, D. A. Chemical and structural investigation of high-resolution patterning with HafSOx. *ACS Appl. Mater. Interfaces* **2014**, *6*, 2917−2921.
(61) Oleksak, R.; Herman, G. Characterization of high-resolution HafSOx inorganic resists. *Proc. SPIE* **2014**, 90483H.
(62) Jackson, M. N.; Kamunde-Devonish, M. K.; Hammann, B. A.; Wills, L. A.; Fullmer, L. B.; Hayes, S. E.; Cheong, P. H. Y.; Casey, W. H.; Nyman, M.; Johnson, D. W. An overview of selected current

approaches to the characterization of aqueous inorganic clusters. *Dalton Trans.* **2015**, *44*, 16982−17006.

(63) Luo, F.; Manichev, V.; Li, M.; Mitchson, G.; Yakshinskiy, B.; Gustafsson, T.; Johnson, D.; Garfunkel, E. Helium ion beam lithography (HIBL) using HafSOx as the resist. *Proc. SPIE* **2016**, *9779*, 977928.

(64) Cattoni, A.; Mailly, D.; Dalstein, O.; Faustini, M.; Seniutinas, G.; Rosner, B.; David, C. Sub-10 nm electron and helium ion beam lithography using a recently developed alumina resist. *Microelectron. Eng.* **2018**, *193*, 18−22.

(65) Zanchetta, E.; Giustina, G. D.; Grenci, G.; Pozzato, A.; Tormen, M.; Brusatin, G. Novel hybrid organic−inorganic spin-on resist for electron-or photon-based nanolithography with outstanding resistance to dry etching. *Adv. Mater.* **2013**, *25*, 6261−6265.

(66) Ghorbani-Asl, M.; Enyashin, A. N.; Kuc, A.; Seifert, G.; Heine, T. Defect-induced conductivity anisotropy in MoS_2 monolayers. *Phys. Rev. B: Condens. Matter Mater. Phys.* **2013**, *88*, 245440.

(67) Zhou, W.; Zou, X.; Najmaei, S.; Liu, Z.; Shi, Y.; Kong, J.; Lou, J.; Ajayan, P. M.; Yakobson, B. I.; Idrobo, J. C. Intrinsic structural defects in monolayer molybdenum disulfide. *Nano Lett.* **2013**, *13*, 2615−2622.

(68) Kang, N.; Paudel, H. P.; Leuenberger, M. N.; Tetard, L.; Khondaker, S. I. Photoluminescence quenching in single-layer MoS_2 via oxygen plasma treatment. *J. Phys. Chem. C* **2014**, *118*, 21258−21263.

(69) Fox, D. S.; Zhou, Y.; Maguire, P.; O'Neill, A.; O'Coileain, C.; Gatensby, R.; Glushenkov, A. M.; Tao, T.; Duesberg, G. S.; Shvets, I. V.; et al. Nanopatterning and electrical tuning of MoS_2 layers with a subnanometer helium ion beam. *Nano Lett.* **2015**, *15*, 5307−5313.

(70) Deng, Y.; Wang, G.; Qiu, Y.; He, D.; Lin, J.; He, J. Nanopatterning of a monolayer molybdenum disulfide with sub-nanometer helium ion beam: considering its shape, size and damage. *Nanotechnology* **2020**, *31*, 345302−345307.

(71) Del Re, R.; Passarelli, J.; Sortland, M.; Cardineau, B.; Ekinci, Y.; Buitrago, E.; Neisser, M.; Freedman, D. A.; Brainard, R. L. Low-line edge roughness extreme ultraviolet photoresists of organotin carboxylates. *J. Micro/Nanolithogr., MEMS, MOEMS* **2015**, *14*, 043506.

(72) Sortland, M.; Hotalen, J.; Del Re, R.; Passarelli, J.; Murphy, M.; Kulmala, T. S.; Ekinci, Y.; Neisser, M.; Freedman, D. A.; Brainard, R. L. Platinum and palladium oxalates: positive-tone extreme ultraviolet resists. *J. Micro/Nanolithogr., MEMS, MOEMS* **2015**, *14*, 043511.

(73) Bae, W. J.; Trikeriotis, M.; Sha, J.; Schwartz, E. L.; Rodriguez, R.; Zimmerman, P.; Giannelis, E. P.; Ober, C. K. High refractive index and high transparency HfO_2 nanocomposites for next generation lithography. *J. Mater. Chem.* **2010**, *20*, 5186−5189.

(74) Reddy, P. G.; Thakur, N.; Lee, C. L.; Chien, S. W.; Pradeep, C. P.; Ghosh, S.; Tsai, K. Y.; Gonsalves, K. E. Heavy metal incorporated helium ion active hybrid non-chemically amplified resists: Nanopatterning with low line edge roughness. *AIP Adv.* **2017**, *7*, 085314.

(75) Sharma, S. K.; Reddy, P. G.; Moinuddin, M. G.; Ghosh, S.; Pradeep, C. P.; Gonsalves, K. E. Helium ion active hybrid non-chemically amplified resist (n-CAR) for sub-10 nm patterning applications. *Proc. SPIE* **2018**, *10584*, 1058409.

(76) Lewis, S. M.; Hunt, M. S.; DeRose, G. A.; Alty, H. R.; Li, J.; Wertheim, A.; De Rose, L.; Timco, G. A.; Scherer, A.; Yeates, S. G.; Winpenny, R. E. P. Plasma-etched pattern transfer of sub-10 nm structures using a metal−organic resist and helium ion beam lithography. *Nano Lett.* **2019**, *19*, 6043−6048.

(77) Xu, H.; Sakai, K.; Kasahara, K.; Kosma, V.; Yang, K.; Herbol, H. C.; Odent, J.; Clancy, P.; Giannelis, E. P.; Ober, C. K. Metal−organic framework-inspired metal-containing clusters for high-resolution patterning. *Chem. Mater.* **2018**, *30*, 4124−4133.

(78) Li, L.; Chakrabarty, S.; Jiang, J.; Zhang, B.; Ober, C.; Giannelis, E. P. Solubility studies of inorganic−organic hybrid nanoparticle photoresists with different surface functional groups. *Nanoscale* **2016**, *8*, 1338−1343.

(79) Kumar, R.; Chauhan, M.; Moinuddin, M. G.; Sharma, S. K.; Gonsalves, K. E. Development of nickel-based negative tone metal oxide cluster resists for sub-10 nm electron beam and helium ion beam lithography. *ACS Appl. Mater. Interfaces* **2020**, *12*, 19616−19624.

(80) Lewis, S.; DeRose, G.; Hunt, M.; Scherer, A.; Yeates, S.; Winpenny, R. E. P.; Alty, H. R.; Werthiem, A.; Li, J.; Fowler, T.; Lee, S.; Muryn, C. A.; Timco, G. A. Design and implementation of the next generation electron beam resists for the production of EUVL photomasks. *Proc. SPIE* **2018**, 108100N.

(81) Brongersma, M. L.; Halas, N. J.; Nordlander, P. Plasmon-induced hot carrier science and technology. *Nat. Nanotechnol.* **2015**, *10*, 25.

(82) Liu, J.; Kutty, R. G.; Zheng, Q.; Eswariah, V.; Sreejith, S.; Liu, Z. Hexagonal boron nitride nanosheets as high-performance binder-free fire-resistant wood coatings. *Small* **2017**, *13*, 1602456.

(83) Ober, C. K.; Xu, H.; Kosma, V.; Sakai, K.; Giannelis, E. P. EUV photolithography: resist progress and challenges. *Proc. SPIE* **2018**, 1058306.

(84) Sharma, S. K.; Moinuddin, M. G.; Yogesh, M.; Sharma, S.; Sahani, M.; Ghosh, S.; Gonsalves, K. E. Focusing on nanoparticles based photomultiplier in n-CARs. *Proc. SPIE* **2020**, 113261C.

■ NOTE ADDED AFTER ASAP PUBLICATION

This paper was published on November 24, 2020. Due to production error, a reference citation was missing in the text and a unit of measurement was incorrect. The corrected version was reposted on November 25, 2020.

https://dx.doi.org/10.1021/acsaelm.0c00627
ACS Appl. Electron. Mater. XXXX, XXX, XXX−XXX